Efficient Time Sampling Strategy for Transient Absorption Spectroscopy

Juhyeon Kim, Joshua Multhaup, Mahima Sneha, and Adithya Pediredla

Abstract—Transient absorption spectroscopy (TAS) is a field of study that investigates the dynamic process of chemical compounds. Thanks to the recent emergence of ultrafast pulsed lasers, TAS now extends its reach to studying photochemical reactions occurring within few femtosecond to nanosecond timescales. With ultrafast TAS, changes in sample absorbance or transmittance over time following excitation by pulsed light can be measured at a high temporal resolution -tens of femtoseconds. An application of ultrafast TAS is lifetime measurement for fluorescence decay. However, due to various noise sources (sensor noise, shot noise, unintended photochemical reactions, etc.) during measurement, obtaining a reliable lifetime value often necessitates extensive repetition resulting in experiments lasting several hours. In this paper, we introduce an effective time sampling strategy tailored for lifetime measurement from noisy transient signals. We start with a well-established non-linear curve fitting algorithm and demonstrate that sampling time shifts that maximize the signal derivative ($t = \tau$) will minimize the variance in lifetime estimation. Additionally, we reduce the number of parameters by normalization to ensures the correctness of our algorithm. We demonstrate using simulation that our proposed method outperforms conventional time sampling or normalization methods across various conditions. Especially, we found that proposed method gives same error with $5.5\times$ less samples compared to the common TAS measurement strategy that uses exponential time sampling with full parameter curve-fitting. Moreover, through real-world TAS measurements, we show that our technique results in $2 - 8\times$ less standard deviation compared to baseline methods. We expect that our algorithm will be valuable not only for researchers who use TAS but also for researchers across various fields who use time-gated transient cameras for lifetime analysis.

Index Terms—Transient Absorption Spectroscopy, Transient Imaging, Femtochemistry, Non-linear Curve Fitting

1 Introduction

Recent advances in imaging systems, especially the advent of ultrashort tunable lasers in 1990s [1], have catalyzed the emergence of a new research domain for chemistry researchers, *femtochemistry*. Femtochemistry has allowed chemists to investigate ultrafast chemical processes happening within tens of femtoseconds to nanoseconds. A quintessential application of femtochemistry is ultrafast transient absorption spectroscopy (TAS), which has offered a deeper understanding of the transient dynamics of photochemical reactions.

TAS employs a pump-probe scheme where a high intensity pump pulse (typically in UV-Visible wavelength range) is used to excite molecules from ground to higher lying electronic energy states. The pump-induced changes to the system are then followed by a broadband probe pulse (varying from X-rays to mid-IR range). In TAS, the data is typically plotted as change in absorbance which indicate the absorbance difference between pump-on and pump-off probe spectra. To attain a time-resolved profile, this procedure is iterated with various time delays between the pump and probe pulses. This procedure is similar to measuring transients with time-gated cameras by shifting the time gates [2]. The excited state of a molecule can decay by various radiative (such as fluorescence and phosphorescence) and non-radiative processes. The time-resolved measurements allow us to estimate the excited state lifetimes by fitting the kinetic traces of the integrated signal to exponential decay functions.

However, the transient profile obtained from TAS is inherently imperfect, as each observation is susceptible to various sources of noise. Unintended photochemical or photothermal reactions may occur, alongside traditional imaging noise such as shot noise, dark current noise, and read noise, all of which contribute to the degradation of estimated lifetime reliability. Existing approach to mitigate these challenges is to increase the number of time samples and exposure duration (repetitions) per time sample. This results in a typical TAS measurement taking 30 minutes to several hours [3–6], while the exact data collection time may depend on the target signal-to-noise ratio or experimental condition. Often the long exposure times can lead to photo or air degradation of the sample. Moreover, when triplet states are involved, the system needs to remain deoxygenated during the course of measurement, which becomes difficult to maintain for longer duration. Speeding the experimental measurement time will allow researchers to do more data collection in shorter time thereby accelerating scientific research and discovery.

To address this challenge, rather than increasing the number of samples, we propose a meticulously crafted time-sampling and data processing algorithm to minimize the uncertainty of the estimated lifetime. Through simulation, we found that our method reduces RMSE (root mean square error) by $4\times$ compared to one of the widely used TAS measurment strategy (exponential sampling with full parameter curve-fitting), which empirically translates to $5.5\times$ less sample to achieve same RMSE. We also observed that

- *J. Kim and A. Pediredla are with the Department of Computer Science, Dartmouth College, Hanover, NH, 03755. J. Multhaup and M. Sneha are with the Department of Chemistry, Dartmouth College, Hanover, NH, 03755.*
- *E-mail: juhyeon.kim.gr@dartmouth.edu*
- *Project page : https://juhyeonkim95.github.io/project-pages/transient_absorption_spectroscopy/*

our method reduces standard deviation by $2-8\times$ for real TAS measurements. While our algorithm was developed to expedite TAS procedures, we anticipate its utility extending to researchers across various domains requiring analysis of exponentially decaying models such as Yu et al. [2].

Here is brief overview of our algorithm: Starting from conventional non-linear least square methods, we derive a condition that minimizes variance of estimated parameters. Assuming independent and identically distributed noise, we show that the optimal sampling point is the value that maximizes function derivative with respect to the parameter that we are interested in. We also propose data normalization that reduces the number of degrees-of-freedom in the parametric model and show that it ensures correctness of our technique. We demonstrate the effectiveness of our algorithm using both simulations and real-world data from TAS measurements. A step-by-step algorithm is provided in Sec. 5.5. Readers solely interested in the algorithmic details may directly navigate to Sec. 5.5.

2 Related Work

2.1 Transient Absorption Spectroscopy

Transient absorption spectroscopy has widespread applications in the study of ultrafast processes [7–14]. TAS can be used to measure elemental processes such as electron transfer [12], conformational change [15], chemical reactions [16] or solvation [17], and it is also used to explore the spectrodynamical properties of photochemical and photobiological systems [7].

In this paper, we focus on the excited state dynamics of 4CzIPN. The excited state dynamics of thermally activated delayed fluorescence (TADF) molecules has been of great interest for the growth of organic light-emitting diodes (OLEDs) [11, 18, 19]. Its high efficiency through delocalized intramolecular charge has been discussed [11]. 4CzIPN does show the properties of an extremely highly efficient TADF molecule [11–13]. Most recent studies show its usage as (organo)photoredox catalysts in C(sp^3)-H bond functionalization [12], or its use as a corresponding anionic and cationic radical in the utilization of isonitriles as alkyl radical precursors in light-mediated hydro- and deuterodeamination reactions [13].

2.2 Data Analysis and Mathematical Modeling

A critical component of transient spectroscopy is not only the accurate measurement of the transient signal, but also analysis of observed datasets, commonly referred to as *chemometrics* [20]. Its primary aim is the statistical analysis and mathematical modeling of chemical data. Chemometrics has facilitated the comprehension of complex systems, enabling the interpretation of chemical phenomena in various field including photochemistry [21], chromatography [22–24] and also transient spectroscopy [7, 25].

2.2.1 Mathematical Modeling for Data Explanation

Mathematical modeling to explain the observed data could be largely categorized into two groups [26]. First is hard-modeling or parametric modeling, which assumes specific mathematical function for data interpretation. Such approach is useful if one have strong prior knowledge on certain phenomenon, such as global lifetime analysis on fluorescence phenomenon. Another group is soft-modeling or model-free methods which do not make assumptions about the specific type of function so that are more applicable to general cases. Additionally, hybrid methods exist, which utilize different models for the temporal and spectral axes.

When the data measured is for a mixture of different chemicals or energy state transitions exhibiting varying spectral profiles rather than being globally consistent, multivariate curve resolution (MCR) methods come into play [27]. Mathematically, MCR represents a superposition of single separable models, but it entails higher complexity as it necessitates considering the mixing coefficient (or spectra profile) of each model. Variations of MCR, including multivariate curve resolution by alternating least squares (MCR-ALS)[28] or employing weighted strategies (MCR-WALS)[26], also exist.

In this study, our primary focus lies on single-parametric models (or mixtures of two, which could be approximated as single for certain time ranges) with exponential decay. This is particularly relevant for many fluorescence dynamics, including the case of 4CzIPN.

2.2.2 Curve-fitting Algorithm for Parametric Modeling

To estimate parameters for the parametric model, we need to rely on curve-fitting algorithms [29, 30], a subject widely explored in the field of statistics. The *least squares* method would be the most commonly employed method, that aims to minimize the squared error between observations and values derived from the parametric model. While the least squares method for linear models has a closed-form solution, we require an alternate approach for non-linear models.

A commonly utilized algorithm for non-linear least squares is an iterative method that updates function parameters until convergence, guided by the gradient of the parametric function with respect to its parameters. Typical examples include the Gauss-Newton or Levenberg-Marquardt algorithms [31], which will be elaborated in Sec. 5.1.

2.2.3 Noise Modeling

Observations are inevitably affected by noise, which can degrade the performance of curve-fitting algorithms. It is often assumed that this noise is independent and identically distributed (*iid*), a condition known as *homoscedastic* noise. However, there also exists *heteroscedastic* noise, where the variance is not constant. Sensor read noise, encompassing thermal noise, source follower noise, and banding pattern noise, is typically modeled using independent Gaussian noise [32, 33]. Conversely, shot noise in single-photon imaging systems serves as a common example of heteroscedastic noise, following a Poisson distribution. Noise modeling can even be more complex if it is correlated over time or spectra [26].

In our work, we mostly focus on Gaussian homoscedastic noise based on real-data observations. However, if the noise distribution is known, we could extend our model to heteroscedastic case, and in Fig. 5, we show a few examples for different noise distributions.

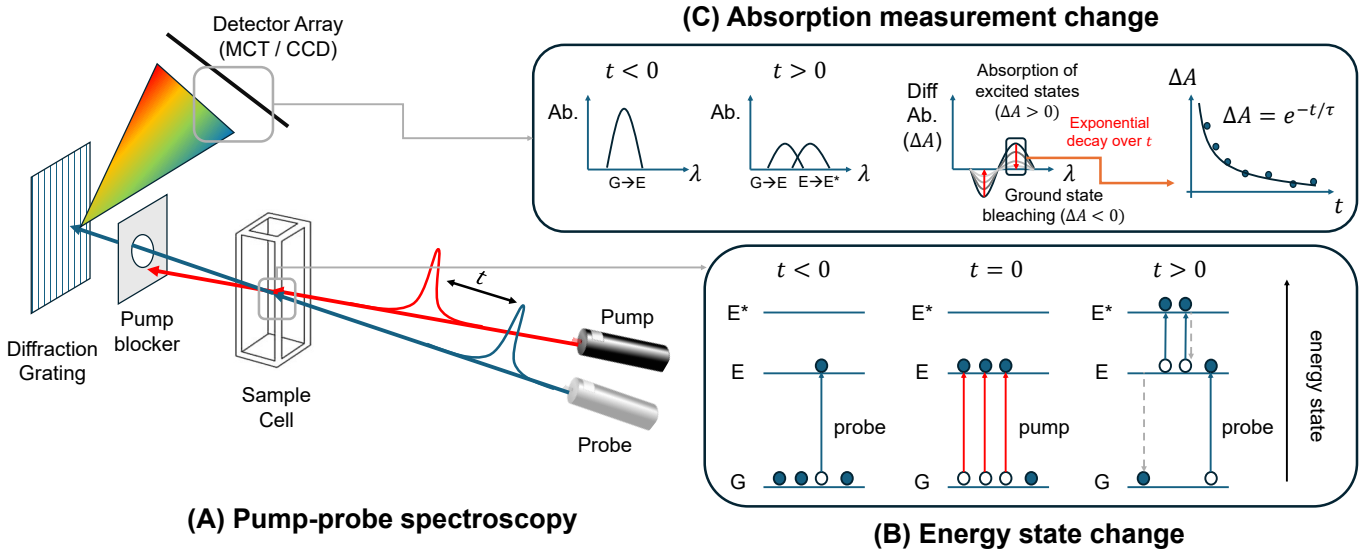

Fig. 1. (A) Illustration of transient absorption spectroscopy. We use a pump pulse to excite the electrons and a probe pulse after a time delay of t to measure the absorption across wavelengths. (B) For $t < 0$, i.e., with no pump pulse, only the probe pulse excites electrons from the ground state (G) to the excited state (E). We show the corresponding absorption spectrum as the first plot in (C). At $t = 0$, pump pulse excites large numbers of the electrons to get E state. If we pass the probe laser at $t > 0$, fewer electrons are at the ground state, so absorption of G→ E is reduced (due to ground state bleaching by pump pulse). On the other hand, the probe excites electrons to another state, E*, which creates a new peak in the absorption spectra (absorption of the excited state). The second plot in (C) shows the new absorption spectrum. By computing the difference in the absorption spectra measured at pump off and $t > 0$ (pump-on), one can calculate differential absorbance ΔA, shown as third plot in (C). Lack of ground state electrons (ground state bleaching) results in $\Delta A < 0$, while absorption of excited state shows as $\Delta A > 0$. The differential absorption decays exponentially, and the decay parameter τ is called the lifetime of the state, which gives us information on the speed of a chemical reaction.

2.3 Optimal Sampling Strategy for Curve Fitting

The reliability of reconstructed function parameters is influenced by the noise profile, fitting algorithm, but also the selection of samples, which necessitates well-designed strategy for the sampling process.

In the field of statistics, several works have addressed this problem for linear regression models [34–38]. These studies aim to determine the sampling frequency of each covariate that minimizes the L2 loss between the latent ground truth parameter β^* and the estimated parameter $\hat{\beta}$, quantified by $\mathbb{E}[\|\hat{\beta} - \beta^*\|^2]$. This problem statement shares similarities with the multi-arm bandit problem in reinforcement learning [37], showcasing an exploration-exploitation trade-off. A common approach involves finding an A-optimal solution that minimizes the trace of the covariance matrix.

Our paper aligns with the objective function of previous works, seeking an optimal sampling strategy that minimizes $\mathbb{E}[\|\hat{\beta} - \beta^*\|^2]$. However, there are several distinctions. First, our sampling domain does not have constraints, unlike previous papers. In other words, we have to determine where to sample rather than how many times to sample each covariate. Second, our parametric model is a non-linear function without a closed-form solution, rendering the optimization process more complex. To address these challenges, we introduce a single-point approximation method (Sec. 5.2), resulting in a solution that we prove is empirically optimal.

3 Transient Absorption Spectroscopy

Transient absorption spectroscopy (TAS) is a widely employed technique in chemistry for studying the dynamics of chemical reactions [11–13]. TAS is a pump-probe technique and is illustrated in Fig. 1. This technique utilizes two types of pulsed lasers: a pump pulse, commonly narrow bandwidth with IR wavelength (e.g. 425 nm) to excite electrons and a probe pulse, commonly broadband (known as white light continuum) to measure absorption with a delay of t [14, 39, 40]. The probe pulse could also encompass other wavelength regions, such as mid-IR which will in turn probe pump induced dynamics through vibrational signatures of ground and excited molecules. After passing through the sample, the probe pulse is directed to a diffraction grating which disperses the probe light on a detector array. The intensity difference between the reference laser beam and the beam passing through the sample is used to generate the absorption spectrum. The detector array are typically implemented with Mercury Cadmium Telluride (MCT) array or charge-coupled device (CCDs) [12].

The detailed energy-level process of TAS is depicted in Fig. 1-(B, C) [19, 41]. Initially, for $t < 0$, the majority of electrons reside in the ground state energy level (G). Probe pulse excites the ground state molecules only, and the detector therefore records the ground state absorption spectra (G→E). Upon the arrival of the high-intensity pump pulse at $t = 0$, a small fraction of the molecules are excited to a higher energy level (G→E). At $t >= 0$, the probe pulse excites both ground state moelcules (G→E) and excited state molecules (E→E*), which have different energies, thus they appear at different wavelengths on the spectra. However,

a reduced ground state absorption occurs due to the depopulation of ground state molecules by the pump pulse, a phenomenon known as *ground state bleaching*.

By calculating the absorbance difference between $t > 0$ (pump-on) and any time before the pump pulse (pump-off), we can compute a differential absorbance ΔA spectrum which manifests dynamics induced by the pump pulse.

$$\Delta A(\lambda, t) = A_{\text{pump}-\text{on}}(\lambda, t) - A_{\text{pump}-\text{off}}(\lambda) \tag{1}$$

Ground state bleaching manifests as $\Delta A < 0$, while excited state absorption manifests as $\Delta A > 0$. Additionally, phenomena such as stimulated emission ($\Delta A < 0$) or product absorption ($\Delta A > 0$) may occur, although they are not illustrated in Fig. 1-(B). In ultrafast TAS spectroscopy, the pump off measurement is generally taken on a shot-by-shot basis by using a chopper which blocks every other pump pulse at each sampling time t.

In the absence of a quencher, molecules will return to the ground state, and the deviation of the differential absorbance gradually diminishes over time. Consequently, the peak attributed to ground state bleaching or excited state absorption in Fig. 1-(C) decays as the spectra is measured at increasing time delays t. For certain cases, the population decay should theoretically follow an exponential function ($e^{-t/\tau}$) [26, 42, 43] with a specific constant τ, known as the *lifetime*. The investigation of the lifetime of a excited state can give information on the speed and efficiency of a chemical reaction and the influence of experimental conditions such as temperature, solvent environment and others. It is also used to gain information on the reaction mechanism, molecular interactions and the transitions states [44].

4 Problem Statement

Since exponential decay may happen for various energy state transitions or different chemical compounds, $\Delta A(\lambda, t)$ is often represented as a sum of exponential decays in Global Lifetime Analysis (GLA) [26],

$$\Delta A(\lambda, t) = \sum_{k=1}^{K} A_k(\lambda) e^{-t/\tau_k}. \tag{2}$$

Here, K is the size of the basis expansion, $A_k(\lambda)$ is the coefficient related to each wavelength, and τ_k is the lifetime of each exponential decay. Since specific reaction only shows meaningful value for certain wavelength regions, we often integrate $\Delta A(\lambda, t)$ over λ for the region of interest, reducing ΔA to a function of t alone. Such global analysis assumes hard modeling of exponential decay but is a powerful tool if prior determination on the number of exponentials is possible.

In this paper, we consider *monoexponential* or *biexponential kinetics* where $K = 1, 2$. Biexponential kinetics is usually composed of two lifetimes, prompt τ_p and delayed τ_d which govern different energy state transitions,

$$\Delta A(t) = A_p e^{-t/\tau_p} + A_d e^{-t/\tau_d}. \tag{3}$$

In general, $\tau_d \gg \tau_p$ (τ_p is in nanoseconds scale, τ_d is in microseconds to even seconds scale [45]), and assuming that we are only interested in τ_p, we can approximate the second term as a constant, which makes the target parametric function as

$$\Delta A(t) = A_p e^{-t/\tau_p} + A_d. \tag{4}$$

Note that such model inherently covers monoexponential case. For notation brevity, we will use the following model instead:

$$I(t) = A e^{-t/\tau} + B. \tag{5}$$

In short, our goal is to find an efficient time sample sequence $[t_i]_{i=1}^{M}$, given the constraint on the number of measurement M, so that estimated lifetime using parametric model in Eq. (5) gives an accurate value after non-linear curve fitting.

5 Proposed Solution

In this section, we will delineate the proposed method to reduce variance of estimated lifetime. We will first examine how non-linear curve fitting algorithms work and derive an optimal sampling strategy based on approximations. We also show normalization process which has empirically guaranteed correctness of our method.

5.1 Non-linear Curve Fitting

Curve fitting is a well-known problem in statistics, where the objective is to find the parameters β of a target function $f(x, \beta)$ that best describes a set of M data pairs (x_i, y_i). A commonly used method is *least-square* method which aims to find an optimal $\hat{\beta}$ that minimize the sum of the squares of the deviations $S(\beta)$:

$$\hat{\beta} \in \arg\min_{\beta} S(\beta) = \arg\min_{\beta} \sum_{i=1}^{M} \left(y_i - f(x_i, \beta)\right)^2. \tag{6}$$

While closed-form solutions exist for simple cases like linear models, they are generally not feasible for non-linear models. An iterative approach is often employed for solving Eq. (6) in the non-linear case.

Starting from an initial guess on β, we iteratively update β to $\beta + \delta$. To determine the δ, we use a first-order approximation:

$$f(x, \beta + \delta) = f(x, \beta) + \delta^T \nabla f \tag{7}$$

where $\nabla f = \frac{\partial f(x,\beta)}{\partial \beta}$ is a gradient of f regards to β. Using this approximation, we can represent Eq. (6) with $\beta + \delta$ as

$$S(\beta + \delta) \approx \|\mathbf{y} - \mathbf{f}(\beta) - \mathbf{J}\delta\|^2 \tag{8}$$

$$= (\mathbf{y} - \mathbf{f}(\beta))^T (\mathbf{y} - \mathbf{f}(\beta)) - 2(\mathbf{y} - \mathbf{f}(\beta))^T \mathbf{J}\delta + \delta^T \mathbf{J}^T \mathbf{J}\delta, \tag{9}$$

where $\mathbf{J}$ is Jacobian matrix with row of $\mathbf{J}_i = \frac{\partial f(x_i,\beta)}{\partial \beta}$, $\mathbf{f}(\beta) = [f(x_i, \beta)]_{i=1}^{M}$ and $\mathbf{y} = [y_i]_{i=1}^{M}$. Taking the derivative of above equation with respect to δ and setting it to zero yields:

$$\left(\mathbf{J}^T \mathbf{J}\right) \delta = \mathbf{J}^T \left(\mathbf{y} - \mathbf{f}(\beta)\right). \tag{10}$$

We can then calculate δ by taking an inverse of $\left(\mathbf{J}^T \mathbf{J}\right)$. Such method is known as *Gauss-Newton* method. *Levenberg-Marquardt* method [31] is a variation of Gauss-Newton method that introduces a damping factor λ

$$\left(\mathbf{J}^T \mathbf{J} + \lambda \text{diag}\left(\mathbf{J}^T \mathbf{J}\right)\right) \delta = \mathbf{J}^T (\mathbf{y} - \mathbf{f}(\beta)). \tag{11}$$

Note that if $\lambda = 0$, it is equivalent to Gauss-Newton method.

5.2 Finding an Optimal Sampling Distribution for Non-linear Curve Fitting

Assume the target model could be perfectly modeled using a parametric model with latent ground truth parameter β^*. Prior knowledge about the system could help us determine the parametric model, which is true for TAS. However, the actual observation y is not a deterministic value but affected by an uncontrollable error ϵ:

$$y = f(x, \beta^*) + \epsilon. \tag{12}$$

Therefore, even when utilizing the same sampling points, $\hat{\beta}$ may vary from experiment to experiment.

Our goal is to identify optimal sampling points $\mathbf{x} = [x_i]_{i=1}^M$ that minimizes expected error with the ground truth parameter:

$$\hat{\mathbf{x}} \in \arg\min_{\mathbf{x}} \mathbb{E}[\|\hat{\beta} - \beta^*\|^2], \tag{13}$$

or, if we are only interested in the jth component of β:

$$\hat{\mathbf{x}} \in \arg\min_{\mathbf{x}} \mathbb{E}[\|\hat{\beta}_j - \beta_j^*\|^2]. \tag{14}$$

However, directly solving the above equation is not feasible, except for simple cases, as $\hat{\beta}$ is obtained through an iterative process. Therefore, we will explore an approximate approach to address this challenge.

Instead of considering all of the sampled points at once, we consider the effect of a single additional sample at the specific point as illustrated in Fig. 2. The blue dots and the blue line represent current samples and fitted curve, while the red dot indicates the new sample. To incorporate this new sample into the curve fitting process, we need to update $\hat{\beta}$ to $\hat{\beta}+\delta$. This can be approximately achieved by modifying Eq. (10):

$$(\nabla f \nabla f^T)\delta = k\epsilon \nabla f. \tag{15}$$

Here ∇f is the gradient with respect to β at x, and k is a constant value that mediates the update rate. Note that the exact $\hat{\beta}$ from the iterative method that includes the new data point would be different from $\hat{\beta} + \delta$. However, this approximation still provides a good insight on understanding variance of $\hat{\beta}$.

A solution to Eq. (15) is

$$\delta = \frac{k}{N}\epsilon(\nabla f)^{-1}, \tag{16}$$

where the inverse operation is applied element-wise and N is the dimensionality.

If δ is large, it indicates that $\hat{\beta}$ undergoes significant changes due to a noisy observation, which is harmful to optimize Eq. (14). Thus, it is desirable to minimize δ. Assuming that ϵ is independent and identically distributed (iid), minimizing δ is equivalent to maximizing ∇f. For Eq. (11), we could get

$$\delta = \frac{k}{N}\epsilon(\nabla f + \lambda)^{-1}, \tag{17}$$

which still supports the advantage of maximizing ∇f.

In conclusion, we can approximately say that to minimize error in $\hat{\beta}_j$, we need more samples at the point that maximizes $(\nabla f)_j$.

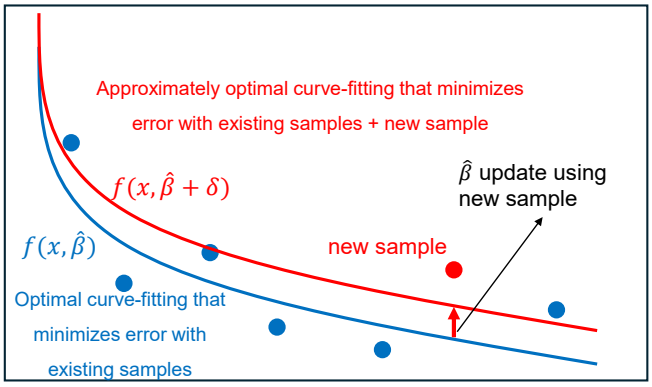

Fig. 2. Single sample approximation. The blue dots are current samples, and the blue line refers to the current fitted curve with $\hat{\beta}$ that optimizes Eq. (6). We update the blue line to the red line as we observe a new sample (red dot). This new parameter is approximated as $\hat{\beta} + \delta$ using Eq. (16).

5.3 Application to Exponential Decay Model

Our latent parametric model follows exponential decay with scale and offset as described in Eq. (5). The actual observation could be modeled as a sum of original ground truth signal and Gaussian-distributed noise.

$$I_o(t) = I(t) + \epsilon = Ae^{-t/\tau} + B + \epsilon \tag{18}$$

From M observations, we could reconstruct the parameters using a non-linear least square method, which was described in Sec. 5.1. Our objective is to identify an optimal sampling strategy for t_i that minimizes the expected error of τ, as our primary interest lies in accurately estimating the lifetime. To exploit the algorithm in Sec. 5.2, we calculate derivative of I with regard to τ which gives:

$$\frac{\partial I}{\partial \tau} = Ae^{-t/\tau}\frac{t}{\tau^2}. \tag{19}$$

To find t that maximizes $\frac{\partial I}{\partial \tau}$, we calculate derivative with regard to t

$$\frac{\partial}{\partial t}\left(\frac{\partial I}{\partial \tau}\right) = \frac{A}{\tau}\left(e^{-t/\tau} - \frac{t}{\tau}e^{-t/\tau}\right), \tag{20}$$

and this has a maximum value at $t = \tau$. Therefore, sampling at time stamps close to the unknown τ will minimize the variance of the estimated τ. While the exact value of τ is unknown, we typically can estimate an approximate lifetime with the knowledge of the molecular structure or prior lifetime experiments of the molecule in a different solvent.

5.4 Reducing Number of Parameters through Data Normalization

In practice, the optimal sampling strategy does not work if we directly apply the sampling algorithm to Eq. (5). This is primarily because sampling only at $t = \tau$ effectively gives only one (but precise) value, which is insufficient given the degrees of freedom in β, leading to failed curve fitting attempts. One solution is to reduce the number of parameters to optimize, and luckily, for the exponential model, we can achieve it.

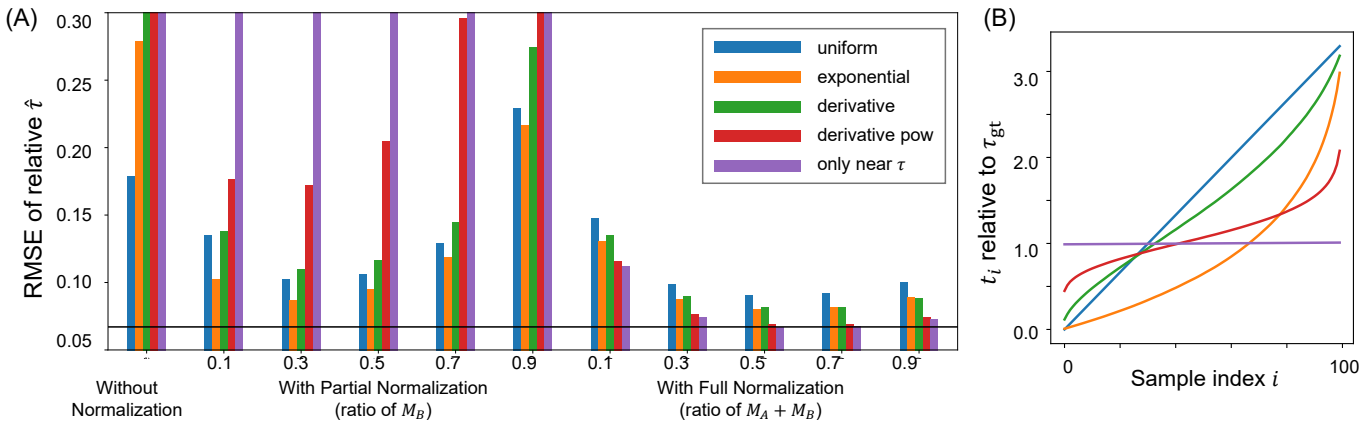

Fig. 3. (A) RMSE of relative error between $\hat{\tau}$ and ground truth τ_{gt} using different sampling method and normalization strategy. Proposed method (sampling only near τ with normalization) shows the best performance compared to other configurations. (B) Averaged and sorted time samples over sample index for each strategy.

We apply the following function normalization:

$$I^{\text{norm}}(t) = \frac{I(t) - B}{A} = e^{-t/\tau} \tag{21}$$

which reduces number of parameters to 1. However, since the values for A and B are unknown, we estimate them using some initial measurements:

$$\langle A + B \rangle = \mathbb{E}[I_{\text{o}}(t = 0)] = \frac{1}{M_A} \sum_{k=0}^{M_A} I_{\text{o}}^k(t = 0), \tag{22}$$

and

$$\langle B \rangle = \mathbb{E}[I_{\text{o}}(t = \infty)] = \frac{1}{M_B} \sum_{k=0}^{M_B} I_{\text{o}}^k(t = \infty) \tag{23}$$

where M_A and M_B are number of samples used for estimating $\langle A + B \rangle$ and $\langle B \rangle$ respectively. Note that the total number of measurements is M, so we can now dedicate $(M - M_A - M_B)$ samples to curve fitting. With these estimators of A and B, we normalize I_{o} as

$$I_{\text{o}}^{\text{norm}}(t) = \frac{I_{\text{o}}(t) - \langle B \rangle}{\langle A + B \rangle - \langle B \rangle}. \tag{24}$$

This normalized observation should follow a single exponential function without any scale or offset. One consideration when evaluating $\langle B \rangle$ is the approximation used for the biexponential model. Since $t = \infty$ gives zero, not B, we can use $t \gg \tau_p$ but $t \ll \tau_d$ instead of ∞.

Empirically, we have found that the optimal sampling strategy described in Sec. 5.2 works as expected under this single parametric model.

5.5 Summary for Optimal Sampling Strategy

We summarize our optimal sampling strategy for estimating accurate τ for exponential model in Eq. (5).

1) Measure the initial value on $t = 0$ with sufficiently many samples for estimate of $A + B$.
2) Measure the constant term on $t = \infty$ (or $t \gg \tau$) with sufficiently many samples for estimate of B.
3) Sample focusing only on a small region near $t = \tau$. We can use approximate estimate for τ in practice.
4) Perform signal normalization as Eq. (24).
5) Optimize processed data with $e^{-t/\tau}$ function using non-linear square curve fitting.

6 Result

We demonstrate the effectiveness of our sampling strategy using both simulation and real-data experiments. However, due to the extensive time required for TAS data acquisition and the cost of conducting the experiments, we show most of the results in simulation, which allows us to thoroughly evaluate the performance of the sampling strategy in various scenarios without the constraints of real-world data collection.

6.1 Simulation experiments

We conducted a comparative analysis of our proposed algorithm against various sampling baselines and normalization techniques through simulation. Our latent target model (Eq. (5)) was parameterized with random values of $A \in [1.0, 2.0]$, $\tau \in [1.0, 3.0]$, and $B \in [0.0, 3.0]$. For notation simplicity, we will drop gt and A, τ, B means gt value if not notated otherwise. Noise ϵ was set to follow a normal distribution of $\mathcal{N}(0, 0.165)$, which reflects noise profile of real TAS observations in Fig. 9. The samples are distributed within the range of $t \in [0, 6]$ with $M = 100$. Following sampling methods are employed:

- uniform : $p(t) = \text{constant}$
- exponential : $p(t) \propto e^{-t/\tau}$
- derivative : $p(t) \propto \frac{\partial}{\partial \tau} e^{-t/\tau} \propto te^{-t/\tau}$
- derivative pow : same to above, but powered by 10.
- only near τ : $p(t) = \text{constant}$ for $t \in [0.99\tau, 1.01\tau]$, otherwise 0 (proposed)

where $p(t)$ is sampling pdf for time t. Overall averaged, distribution of sampled times are visualized in Fig. 3-(B). Here, we used ground truth τ value for sampling pdf, but this is also diversified in Sec. 6.1.1. We also tested three different normalization strategies:

- without normalization : optimize $[A, \tau, B]$ for model of $Ae^{-t/\tau} + B$
- with partial normalization : apply offset subtraction and optimize $[A, \tau]$ for model of $Ae^{-t/\tau}$
- full normalization : apply full normalization as Sec. 5.4 and optimize $[\tau]$ for model of $e^{-t/\tau}$

In normalization-based approaches, we varied the ratios of M_A and M_B to the total number of samples M, to highlight importance of proper normalization. Each experiment was repeated 1000 times with different random seeds. We used `scipy.curve_fit` function for non-linear curve fitting, whose default setting is Levenberg-Marquardt algorithm.

We plot RMSE (root mean square error) of relative error between estimated lifetime $\hat{\tau}$ and ground truth lifetime τ_{gt} in Fig. 3-(A), employing various sampling and normalization strategies outlined earlier. Overall, we found that our proposed sampling method with proper normalization gives the best result among all of the configurations. Regarding sampling strategies, the result was consistent with our interpretation that focusing on τ is helpful (under full normalization). But it deviated a lot if we do not apply normalization, which necessitates the normalization step. Meanwhile, we observed that minimizing the number of parameters with normalization leads to more accurate estimates of τ for all sampling strategies. However, this comes with the caveat that proper normalization is essential. Using too small number of M_A, M_B gives false estimate for A and B which makes data biased after normalization step. On the other hand, if we use too many samples to get accurate estimate of A, B, we cannot dedicate enough samples for curve-fitting which makes the result worse. Our observations indicate that an optimal proportionality holds for $M_A = M_B = 0.35$. This distribution roughly equalizes the sample allocation across three crucial points: $t = 0, t = \infty$, and $t = \tau$, which is essential to evaluate A, B, τ, respectively.

Considering that typical default option used for TAS interpretation is exponential time sampling with full parameter fitting (without normalization) which shows RMSE of 0.28, our proposed method achieves the one-fourth RMSE of 0.07. To achieve same level of RMSE using that typical setting, we found that we need $\times 5.5$ more samples.

6.1.1 *Effect of Using Inaccurate τ for Sampling*

In real-world scenarios, it's often impractical to ascertain the precise value of τ beforehand. Therefore, it's more pragmatic to employ an approximate value, denoted as τ_s, for sampling purposes. To evaluate the effect of inaccurate initial guess, we replicated the previous experiment, maintaining normalization and a ratio of 0.35, while varying the initial guess for τ_s.

The experiment results in Fig. 4 reveal that the performance of our method deteriorates noticeably when τ_s substantially diverges from the ground truth τ_{gt}. However, it still exhibits optimal performance within a moderately wide range, specifically when τ_s/τ_{gt} falls within the interval $[0.5, 1.5]$. Consequently, if an approximate value within $\pm 50\%$ accuracy of the true τ can be utilized, our proposed method proves beneficial.

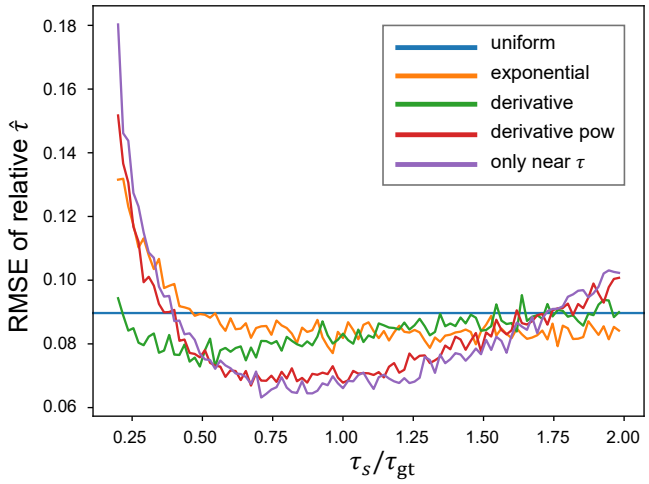

Fig. 4. RMSE of relative error between $\hat{\tau}$ and ground truth τ_{gt} using different initial guess τ_s. It shows that our proposed method shows the lowest RMSE at $\tau_s = \tau_{gt}$ and degrades as τ_s deviates from τ_{gt}. However, compared to other sampling methods, our method shows optimal property over a large range ($\pm 50\%$).

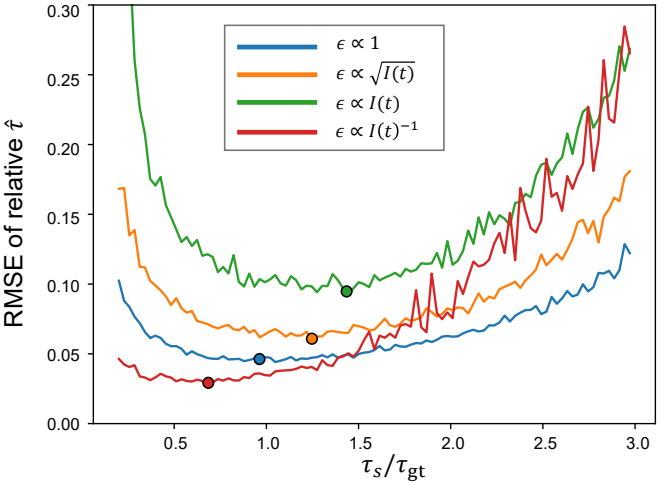

Fig. 5. Result of using heteroscedastic noise. Compared to the homoscedastic case, heteroscedastic noise shows the optimal value at different locations, which is indicated as a circle in the plot.

6.1.2 *Heteroscedastic Noise*

Theoretically, our model is also applicable for the heteroscedastic noise scenarios, provided we know the distribution of ϵ as a function of t. In such instances, instead of maximizing ∇f with respect to t, our objective shifts to finding t that maximizes $\nabla f/\epsilon(t)$.

For instance, if we consider Poisson noise, characterized by variance proportional to $I(t)$, our focus shifts from maximizing $te^{-t/\tau}$ to maximizing $te^{-t/\tau}\sqrt{Ae^{-t/\tau} + B}$. For the previous settings of A and B, the maximum occurs at $t = 1.375\tau$. We present the results for different heteroscedastic noise in Fig. 5 which shows a different optimal point than $t = \tau$.

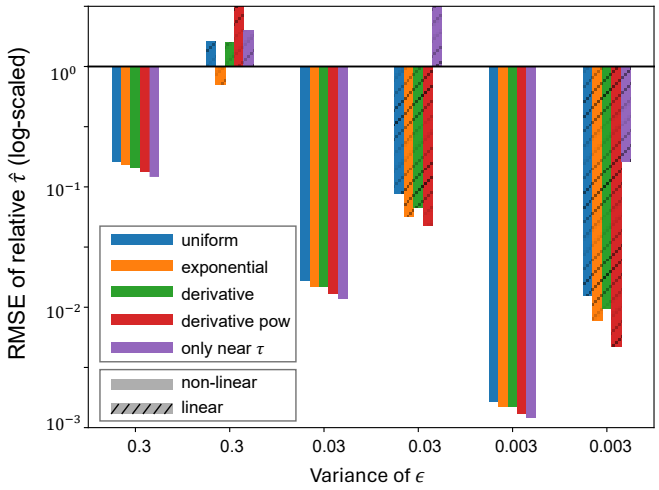

Fig. 6. Result of using linear fitting over various ϵs. Non-linear fitting is more advantageous than linear for all sampling strategies and noise variances. Among the sampling methods, our method gives the best result over different ϵs.

6.1.3 *Comparison with Linear Curve Fitting*

One might question why we do not use simple linear curve fitting after applying the logarithm to the normalized data. Actually, this is a common practice for exponential curve fitting in other fields, such as time constant evaluation in RC circuits. However, we found that such an approach is inferior to non-linear curve fitting in our case, which we demonstrate in Fig. 6 over different sampling methods and different ϵs. The linear curve fitting is inferior as $\log$ exaggerates the noise or even makes a sample invalid due to negative observation. This effect would be relatively small in electric circuits but is critical for the TAS case where noise variances are significantly larger. We could not find any advantage of using the proposed sampling for the linear model.

6.2 Real TAS experiments

Next, we will experiment with real data for lifetime analysis using TAS. We used 4CzIPN in dichloromethane solvent. 4CzIPN is a typical chemical compound which shows bi-exponential kinetics with prompt lifetime of $20-25\text{ns}$ and delayed lifetime of few μs [46].

We first conduct experiment using an exponentially increasing time sequence for $t \in [0\text{ps}, 8000\text{ns}]$, which is a typical time sampling method used in TAS [3]. The result for $\Delta A(\lambda, t)$ is shown in Fig. 7. For better visualization, we plotted ΔA over wavelength for different time values in Fig. 7-(A). As explained before, we could observe positive and negative peaks in ΔA which decay to zero over time. To show a better temporal profile, we integrate differential absorbance for specific wavelength regions and plot over time in Fig. 7-(B). In region (a), approximately $t \in [0\text{ns}, 0.5\text{ns}]$, pump pulse excites the electrons so that ΔA rapidly decreases. We discard this region for exponential decay fitting. In region (b), approximately $t \in [1\text{ns}, 80\text{ns}]$, prompt decay dominates and ΔA rapidly increase over time. In region (c), approximately $t > 100\text{ns}$, delayed decay dominates and ΔA gradually decreases to zero. One can explicitly notice the difference between prompt and delayed decay by comparing the slope. The total number of samples $M = 100$, but we only used 37 samples $t \in [1\text{ns}, 80\text{ns}]$ where prompt decay dominantly takes place.

TABLE 1: Mean and standard deviation of estimated lifetime for different configuration in real-data.

Configuration	Mean	stdev
Exponential (no norm)	32.85	15.37
Exponential (norm)	21.24	4.19
Proposed (norm)	25.95	**2.49**

In contrast, for our proposed method, we uniformly sampled within the range $t \in [20.5\text{ns}, 21.7\text{ns}]$, which is given from the rough measurement using the existing method (exponential + normalization in Tab. 1). This also aligns with previous knowledge that τ_p lie within $20-25$ ns [46]. To be fair, we also randomly selected 37 samples for the proposed sampling.

In calculating the normalization factors, we averaged the values of 10 samples. Note that B does not represent background noise but rather a constant value arising from delayed exponential decay, as mentioned before. Therefore, it couldn't be directly obtained from $t < 0$. Instead, we approximated it using values around $t = 100\text{ns}$. The experiment was repeated 10 times, and curve fitting was performed for each experiment.

In Fig. 8, we present an example of sampled values for single experiment, alongside curve-fitting outcomes with and without normalization. We excluded curve-fitting for the proposed method without normalization, as it was already proven to not work properly using simulation.

In Tab. 1, we provide the average and standard deviation of estimated τ_p across 10 experiments. The result indicate that employing exponential time sampling without normalization yields the poorest results. However, applying normalization techniques notably enhances the accuracy of estimation. Furthermore, the proposed method exhibits the lowest variance compared to default exponential sampling, underscoring its effectiveness in minimizing variability. Theoretically, they should have exactly same mean, but due to lack of repetition there were some variations.

6.2.1 *Noise profile for real measurements*

To demonstrate that our modeling on noise for simulation was reasonable, we present the noise profile observed in our experiments in Fig. 9. We first show the covariance matrix with respect to time in Fig. 9-(A). We found that error is mostly uncorrelated over time as the covariance matrix shows high diagonal values. Although not perfectly identical across time, the similarity observed suggests that the noise could be approximated as homoscedastic. We also plot the noise distribution of normalized observations in Fig. 9-(B). The distribution aligns well with a Gaussian distribution, with a standard deviation of 0.165, which justifies our simulation setting.

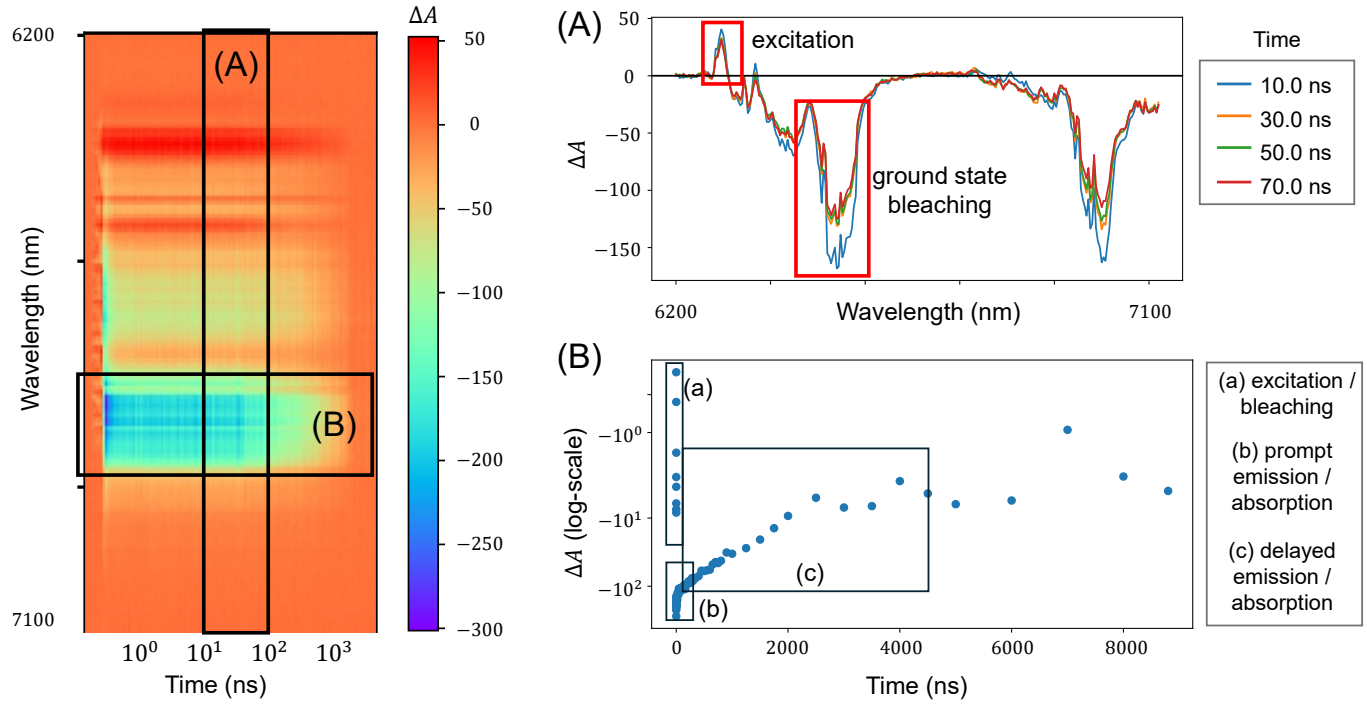

Fig. 7. Result of transient absorption spectroscopy. We measure differential absorbance (ΔA) for each time delay and wavelength and plotted it over wavelength and time in (A) and (B) respectively. We could find ground state bleaching or excitation absorption in (A) and also noticeable difference between prompt/delayed process in (B). Note that the data shown here utilizes a mid-IR probe (see supplementary information).

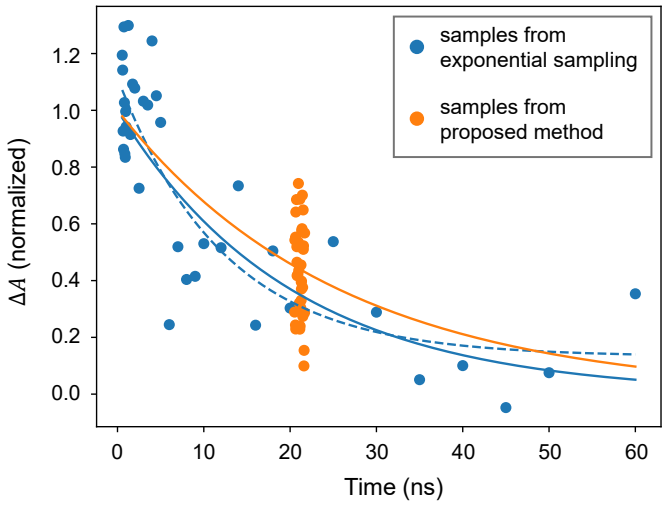

Fig. 8. Example of curve-fitting using exponential time sampling and proposed method for one experiment (we did total 10 repetition). Dotted line refers to curve-fitting without normalization.

7 Conclusion

Ultrafast transient absorption spectroscopy have enabled researchers to resolve femtosecond dynamics in chemical processes. Utilizing pump probe time delays varying from several femtoseconds to nanoseconds or more, crucial information on the different elementary steps can be established such as solvent reorganization time, lifetime kinetics among others. The measurements however often take long time, as the user has to repeat the experiment many times to get a satisfactory signal-to-noise ratio that can be used for parametric model fitting. In this paper, we propose an algorithm that significantly reduces the measurement time using a mathematically robust time-sampling strategy.

We expect there could be various follow-up research of our work - one can extend our method to multiple exponential decays or even other parametric models, or one may consider more complex noise profiles such as correlated noise. Our work can also be improved from a statistical viewpoint. We treated each sample equally for curve fitting, but one can allow duplicates, like the multi-armed bandit problem, and find better solutions. Finally, though we originally targeted our algorithm for TAS users, we expect that our method could be widely applied to other fields that require the analysis of exponential signals.

Acknowledgments

This project is supported by NSF CCF-2403122.

References

[1] P. French, "The generation of ultrashort laser pulses," *Reports on Progress in Physics*, vol. 58, no. 2, p. 169, 1995.

[2] S. Yu, T. Yao, and B. Yuan, "An iccd camera-based time-domain ultrasound-switchable fluorescence imaging system," *Scientific Reports*, vol. 9, no. 1, p. 10552, 2019.

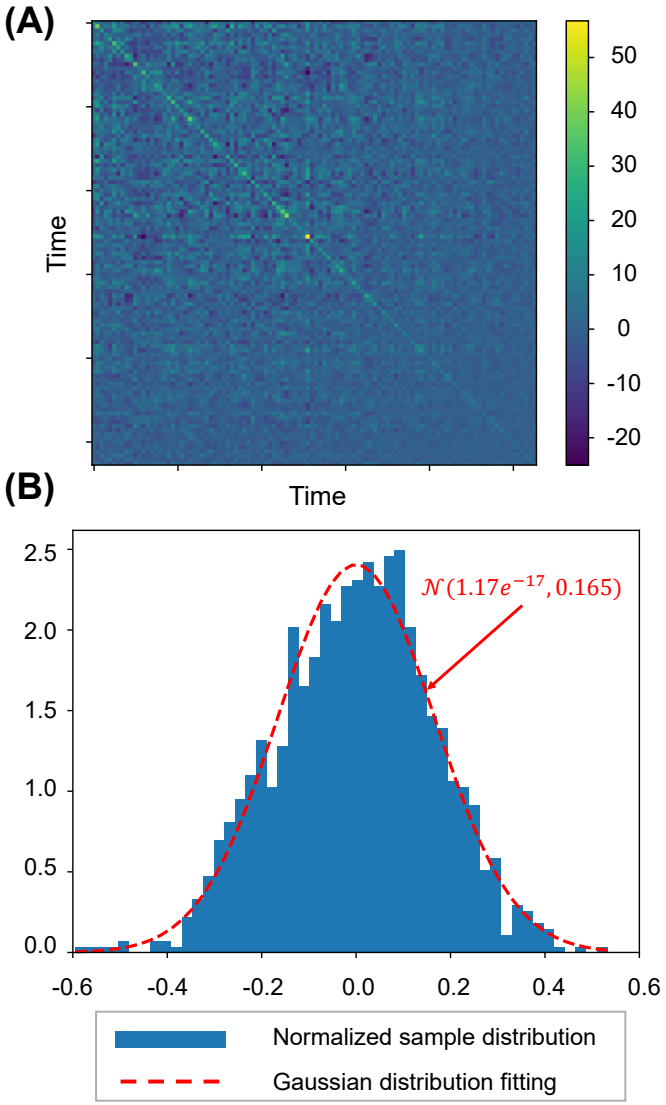

Fig. 9. Error profile of the real measurement. (A) Covariance matrix with regard to time which supports our homoscedastic noise assumption and (B) error on normalized samples which well fits with Gaussian distribution of $\mathcal{N}(0, 0.165)$.

[3] A. Bhattacherjee, M. Sneha, L. Lewis-Borrell, O. Tau, I. P. Clark, and A. J. Orr-Ewing, "Picosecond to millisecond tracking of a photocatalytic decarboxylation reaction provides direct mechanistic insights," *Nature communications*, vol. 10, no. 1, p. 5152, 2019.

[4] K. S. Wilson, A. N. Mapile, and C. Y. Wong, "Broadband single-shot transient absorption spectroscopy," *Optics Express*, vol. 28, no. 8, pp. 11 339–11 355, 2020.

[5] B. Lang, S. Mosquera-Vázquez, D. Lovy, P. Sherin, V. Markovic, and E. Vauthey, "Broadband ultraviolet-visible transient absorption spectroscopy in the nanosecond to microsecond time domain with sub-nanosecond time resolution," *Review of Scientific Instruments*, vol. 84, no. 7, 2013.

[6] B. Lang, "Photometrics of ultrafast and fast broadband electronic transient absorption spectroscopy: State of the art," *Review of Scientific Instruments*, vol. 89, no. 9, 2018.

[7] C. Ruckebusch, M. Sliwa, P. d. Pernot, A. De Juan, and R. Tauler, "Comprehensive data analysis of femtosecond transient absorption spectra: A review," *Journal of Photochemistry and Photobiology C: Photochemistry Reviews*, vol. 13, no. 1, pp. 1–27, 2012.

[8] J.-C. Diels and W. Rudolph, *Ultrashort laser pulse phenomena*. Elsevier, 2006.

[9] T. Elsässer and H. Becker, *Ultrafast hydrogen bonding dynamics and proton transfer processes in the condensed phase*. Springer Science & Business Media, 2013, vol. 23.

[10] V. Sundström, "Femtobiology," *Annu. Rev. Phys. Chem.*, vol. 59, pp. 53–77, 2008.

[11] T. Hosokai, H. Matsuzaki, A. Furube, K. Tokumaru, T. Tsutsui, H. Nakanotani, M. Yahiro, and C. Adachi, "58-2: Revealing the excited-state dynamics of thermally activated delayed flourescence molecules by using transient absorption spectrospy," in *SID Symposium Digest of Technical Papers*, vol. 47, no. 1. Wiley Online Library, 2016, pp. 786–789.

[12] M. Sneha, G. L. Thornton, L. Lewis-Borrell, A. S. Ryder, S. G. Espley, I. P. Clark, A. J. Cresswell, M. N. Grayson, and A. J. Orr-Ewing, "Photoredox-hat catalysis for primary amine α-c–h alkylation: Mechanistic insight with transient absorption spectroscopy," *ACS catalysis*, vol. 13, no. 12, pp. 8004–8013, 2023.

[13] I. Quirós, M. Martín, M. Gomez-Mendoza, M. J. Cabrera-Afonso, M. Liras, I. Fernández, L. Nóvoa, and M. Tortosa, "Isonitriles as alkyl radical precursors in visible light mediated hydro-and deuterodeamination reactions," *Angewandte Chemie*, vol. 136, no. 7, p. e202317683, 2024.

[14] A. Bhattacherjee, M. Sneha, L. Lewis-Borrell, G. Amoruso, T. A. Oliver, J. Tyler, I. P. Clark, and A. J. Orr-Ewing, "Singlet and triplet contributions to the excited-state activities of dihydrophenazine, phenoxazine, and phenothiazine organocatalysts used in atom transfer radical polymerization," *Journal of the American Chemical Society*, vol. 143, no. 9, pp. 3613–3627, 2021.

[15] K. Roy, S. Kayal, V. Ravi Kumar, A. Beeby, F. Ariese, and S. Umapathy, "Understanding ultrafast dynamics of conformation specific photo-excitation: a femtosecond transient absorption and ultrafast raman loss study," *The Journal of Physical Chemistry A*, vol. 121, no. 35, pp. 6538–6546, 2017.

[16] A. Bhattacherjee and S. R. Leone, "Ultrafast x-ray transient absorption spectroscopy of gas-phase photochemical reactions: A new universal probe of photoinduced molecular dynamics," *Accounts of chemical research*, vol. 51, no. 12, pp. 3203–3211, 2018.

[17] X. Tan, T. L. Gustafson, C. Lefumeux, G. Burdzinski, G. Buntinx, and O. Poizat, "Solvation dynamics probed by femtosecond transient absorption spectroscopy: Vibrational cooling and conformational relaxation in s1 trans-4, 4 '-diphenylstibene," *The Journal of Physical Chemistry A*, vol. 106, no. 14, pp. 3593–3598, 2002.

[18] C. Adachi, "Third-generation organic electroluminescence materials," *Japanese Journal of Applied Physics*, vol. 53, no. 6, p. 060101, 2014.

[19] H. Uoyama, K. Goushi, K. Shizu, H. Nomura, and

C. Adachi, "Highly efficient organic light-emitting diodes from delayed fluorescence," *Nature*, vol. 492, no. 7428, pp. 234–238, 2012.
[20] S. D. Brown, T. B. Blank, S. T. Sum, and L. G. Weyer, "Chemometrics," *Analytical chemistry*, vol. 66, no. 12, pp. 315–359, 1994.
[21] S. Liu, S. Kokot, and G. Will, "Photochemistry and chemometrics—an overview," *Journal of Photochemistry and Photobiology C: Photochemistry Reviews*, vol. 10, no. 4, pp. 159–172, 2009.
[22] M. Daszykowski and B. Walczak, "Use and abuse of chemometrics in chromatography," *TrAC Trends in Analytical Chemistry*, vol. 25, no. 11, pp. 1081–1096, 2006.
[23] Ł. Komsta, Y. Vander Heyden, and J. Sherma, *Chemometrics in chromatography*. CRC Press, 2018.
[24] T. S. Bos, W. C. Knol, S. R. Molenaar, L. E. Niezen, P. J. Schoenmakers, G. W. Somsen, and B. W. Pirok, "Recent applications of chemometrics in one-and two-dimensional chromatography," *Journal of separation science*, vol. 43, no. 9-10, pp. 1678–1727, 2020.
[25] L. Blanchet, J. Réhault, C. Ruckebusch, J. P. Huvenne, R. Tauler, and A. de Juan, "Chemometrics description of measurement error structure: Study of an ultrafast absorption spectroscopy experiment," *Analytica chimica acta*, vol. 642, no. 1-2, pp. 19–26, 2009.
[26] S. Brown, R. Tauler, and B. Walczak, *Comprehensive chemometrics: chemical and biochemical data analysis*. Elsevier, 2020.
[27] W. H. Lawton and E. A. Sylvestre, "Self modeling curve resolution," *Technometrics*, vol. 13, no. 3, pp. 617–633, 1971.
[28] R. Tauler, "Multivariate curve resolution applied to second order data," *Chemometrics and intelligent laboratory systems*, vol. 30, no. 1, pp. 133–146, 1995.
[29] M. Maeder and A. D. Zuberbuehler, "Nonlinear least-squares fitting of multivariate absorption data," *Analytical Chemistry*, vol. 62, no. 20, pp. 2220–2224, 1990.
[30] M. Maeder and Y.-M. Neuhold, *Practical data analysis in chemistry*. Elsevier, 2007.
[31] J. J. Moré, "The levenberg-marquardt algorithm: implementation and theory," in *Numerical analysis: proceedings of the biennial Conference held at Dundee, June 28–July 1, 1977*. Springer, 2006, pp. 105–116.
[32] M. Konnik and J. Welsh, "High-level numerical simulations of noise in ccd and cmos photosensors: review and tutorial," *arXiv preprint arXiv:1412.4031*, 2014.
[33] H. Tian, *Noise analysis in CMOS image sensors*. stanFord university, 2000.
[34] D. Nedyalkova and Y. Tillé, "Optimal sampling and estimation strategies under the linear model," *Biometrika*, vol. 95, no. 3, pp. 521–537, 2008.
[35] H. Schreuder and Z. Ouyang, "Optimal sampling strategies for weighted linear regression estimation," *Canadian Journal of Forest Research*, vol. 22, no. 2, pp. 239–247, 1992.
[36] T. Zhang, Y. Ning, and D. Ruppert, "Optimal sampling for generalized linear models under measurement constraints," *Journal of Computational and Graphical Statistics*, vol. 30, no. 1, pp. 106–114, 2021.
[37] X. Fontaine, P. Perrault, M. Valko, and V. Perchet, "Online a-optimal design and active linear regression," in *International Conference on Machine Learning*. PMLR, 2021, pp. 3374–3383.
[38] D. Causeur, "Optimal sampling from concomitant variables for regression problems," *Journal of Statistical planning and Inference*, vol. 128, no. 1, pp. 289–301, 2005.
[39] M. Fushitani, "Applications of pump-probe spectroscopy," *Annual Reports Section" C"(Physical Chemistry)*, vol. 104, pp. 272–297, 2008.
[40] M. Sneha, L. Lewis-Borrell, D. Shchepanovska, A. Bhattacherjee, J. Tyler, and A. J. Orr-Ewing, "Solvent-dependent photochemical dynamics of a phenoxazine-based photoredox catalyst," *Zeitschrift für Physikalische Chemie*, vol. 234, no. 7-9, pp. 1475–1494, 2020.
[41] R. Berera, R. van Grondelle, and J. T. Kennis, "Ultrafast transient absorption spectroscopy: principles and application to photosynthetic systems," *Photosynthesis research*, vol. 101, pp. 105–118, 2009.
[42] M. Maroncelli and G. R. Fleming, "Picosecond solvation dynamics of coumarin 153: The importance of molecular aspects of solvation," *The Journal of chemical physics*, vol. 86, no. 11, pp. 6221–6239, 1987.
[43] P. Coppens, J. Sokolow, E. Trzop, A. Makal, and Y. Chen, "On the biexponential decay of the photoluminescence of the two crystallographically-independent molecules in crystals of [cu (i)(phen)(pph3) 2][bf4]," *The Journal of Physical Chemistry Letters*, vol. 4, no. 4, pp. 579–582, 2013.
[44] W. Becker, "Fluorescence lifetime imaging–techniques and applications," *Journal of microscopy*, vol. 247, no. 2, pp. 119–136, 2012.
[45] V. Goltsev, I. Zaharieva, P. Chernev, and R. J. Strasser, "Delayed fluorescence in photosynthesis," *Photosynthesis research*, vol. 101, pp. 217–232, 2009.
[46] M. A. Bryden, F. Millward, T. Matulaitis, D. Chen, M. Villa, A. Fermi, S. Cetin, P. Ceroni, and E. Zysman-Colman, "Moving beyond cyanoarene thermally activated delayed fluorescence compounds as photocatalysts: an assessment of the performance of a pyrimidyl sulfone photocatalyst in comparison to 4czipn," *The Journal of Organic Chemistry*, vol. 88, no. 10, pp. 6364–6373, 2022.

Juhyeon Kim Juhyeon Kim received his B.S. degree in Electrical and Computer Engineering from Seoul National University in 2019. He also received the M.S. degree in Electrical and Computer Engineering from Seoul National University in 2022. He is currently working on his Ph.D. degree in Computer Science at Dartmouth College. His research focuses on physically-based rendering of special cameras used in computational photography, such as Doppler, Time-of-Flight (ToF) or transient cameras, but also includes other topics in computer graphics such as neural rendering or real-time rendering.

Joshua Multhaup Joshua Multhaup received this B.S. (2018) and M.S (2022) in chemistry at the University Duisburg-Essen in Germany. He is currently a Research Staff Member in the Sneha group at the Dartmouth College. His research interest is the usage of ultra-fast laser systems to study chemical reactions, kinetics with the focus on surfaces, especially water surfaces.

Mahima Sneha Dr. Mahima Sneha obtained her Ph.D. in 2018 from Stanford University under the supervision of Prof. Richard N. Zare. Her thesis work which led to the first-ever direct observation of quantum mechanical interference effects in reactive scattering for the gas phase reaction of H + H2 was a finalist for the Justin Jankunas doctoral dissertation award in Chemical Physics. Following her Ph.D., she secured a Marie Skłodowska-Curie postdoctoral grant to work with Prof. Andrew Orr-Ewing FRS at the University of Bristol in the United Kingdom. At Bristol, she gained expertise in ultrafast condensed phase transient vibrational and electronic spectroscopies and led the research on the mechanistic investigation of photoredox catalytic reactions. Mahima next joined Prof. Poul Petersen's lab at Ruhr University, Germany, as a RESOLV and Alexander von Humboldt fellow to explore water structure and dynamics at zwitterionic polymer-water interfaces with surface-sensitive spectroscopies. Currently, she is an assistant professor in the Chemistry department at Dartmouth College, NH, USA.

Adithya Pediredla is an Assistant Professor in the Department of Computer Science at Dartmouth College, where he leads the Rendering and Imaging Science (RISC) lab, focusing on the intersection of computer graphics, computational imaging, and computer vision. Before this role, he is a postdoctoral fellow at the Robotics Institute, Carnegie Mellon University. He has a Ph.D. from Rice University and a master's degree from the Indian Institute of Science. He won the Ralph Budd Best Engineering Thesis Award for his Ph.D. thesis, the Prof. K. R. Kambati Memorial gold medal, and an innovative student project award from the Indian National Academy of Engineering for his Master's thesis.